UCLA
COMPUTATIONAL AND APPLIED MATHEMATICS

A Numerical Study of the Solution to the 3D Incompressible Navier-Stokes Equations with Forcing Function

Jacob Ystrom
Heinz-Otto Kreiss

July 1998

CAM Report 98-31

Department of Mathematics
University of California, Los Angeles
Los Angeles, CA. 90095-1555

A numerical study of the solution to the 3D incompressible Navier-Stokes equations with forcing function

Jacob Ystrom*
(email: jystrom@math.ucla.edu)
&
Heinz-Otto Kreiss*
(email: kreiss@math.ucla.edu)

Department of Mathematics, UCLA
Los Angeles, CA 90024

July 6, 1998

Abstract

This report describes some numerical experiments for the three-dimensional incompressible Navier-Stokes equations where a forcing function is added to the equations. We study a time-constant forcing as well as a forcing where the random phase is varying smoothly with time. It is demonstrated that the time history of the large scale (low Fourier modes) of the solution reproduces the small scale (high Fourier modes) exponentially fast. We also make perturbations to the time-history, i.e. instead of the correct large scale time history from a reference run we perturb the data. We perturb the amplitude of the Fourier coefficients but not the phase, and we also make a random phase perturbation. The conclusion is the same, the small scales are reproduced except for a part that can be credited the perturbation.

*Supported by the office of Naval research grant no. N00014-93-1-0551; P00005 and no. N00014-98-1-0125

Contents

1 Introduction

In this report we summarize some results for the numerical solution of the three-dimensional incompressible Navier-Stokes equations,

$$\begin{aligned} \boldsymbol{u}_t + (\boldsymbol{u}\cdot\nabla)\boldsymbol{u} + \nabla p &= \boldsymbol{F} + \nu\Delta\boldsymbol{u}, \quad \nu > 0, \quad t \geq 0 && \text{(1.1a)} \\ \nabla\cdot\boldsymbol{u} &= 0, \qquad\qquad t \geq 0, && \text{(1.1b)} \\ \boldsymbol{u} &= \boldsymbol{u}_0(\boldsymbol{x}), \quad p = p_0(\boldsymbol{x}), \quad t = 0, && \text{(1.1c)} \end{aligned}$$

with 2π-periodic boundary conditions and where $\boldsymbol{F} = \boldsymbol{F}(\boldsymbol{x}, t)$ is a prescribed 2π-periodic forcing function. In an earlier report, [1] we studied these equations without forcing. Without a forcing function the kinetic energy comes solely from the initial data and in 3D the time interval where there is balance between large scales and small scales is rather short. In this report we want to study the case of balance between the kinetic energy put into the equations by the forcing function and the high mode dissipation. This report can therefore be considered as a step towards more realistic conditions of homogeneous turbulence. This report uses the same numerical technique, actually the same computer program as in [1]. The notations are the same if not stated differently.

We can expand the solution into Fourier series

$$\boldsymbol{u}(\boldsymbol{x}, t) = \sum_{\boldsymbol{k}} \hat{\boldsymbol{u}}(\boldsymbol{k}, t) e^{i\boldsymbol{k}\cdot\boldsymbol{x}}, \tag{1.2}$$

$$p(\boldsymbol{x}, t) = \sum_{\boldsymbol{k}} \hat{p}(\boldsymbol{k}, t) e^{i\boldsymbol{k}\cdot\boldsymbol{x}}, \tag{1.3}$$

where $\boldsymbol{x} = (x, y, z)^T$, $\boldsymbol{u} = (u, v, w)^T$ and $\boldsymbol{k} = (k_1, k_2, k_3)^T$, $k_i \in \mathcal{N}$. We consider four different type of forcing functions, all have random phase and

a prescribed energy spectrum. Three functions are time independent, they differ in the spectrum shape. The fourth function has a spectrum form coinciding with one of the time independent functions but has a random phase that varies smoothly with time. These forcing functions denoted by

$$\boldsymbol{F} = \boldsymbol{F}_b(\boldsymbol{x}), \quad b \in \{A, B, C\}, \quad \boldsymbol{F} = \boldsymbol{F}_D(\boldsymbol{x}, t),$$

are in Section 2 used to calculate pseudo-stationary turbulent states for the case of $\nu = 1/150$ and $N = 128$. We also make a calculation with $\boldsymbol{F} = \boldsymbol{F}_A$ but with $\nu = 1/300$ and $N = 256$. By pseudo stationary state we mean a state where the kinetic energy and rate of dissipation has reached levels where they not change so much. Typically the kinetic energy and rate of dissipation do not converge to fixed values but instead vary smoothly in time around some nonzero average value. The magnitude of the forcing function is chosen so that the solution is resolved on the grid, based on the smallest scale estimate c.f. [1]. These base-run solutions are denoted by,

$$\boldsymbol{u}_b(\boldsymbol{x}, t), \quad t \geq t_0, \quad b \in \{A, B, C, D, E\},$$

and they are in Section 3 used to make playback-runs. That is, we calculate solutions to the small scale part of Navier-Stokes equations c.f. [1],

$$\begin{aligned} &\boldsymbol{u}_t^{II} + (((\boldsymbol{u}^I + \boldsymbol{u}^{II}) \cdot \nabla)\boldsymbol{u}^{II})^{II} + \\ &\quad ((\boldsymbol{u}^{II} \cdot \nabla)\boldsymbol{u}^I)^{II} + \nabla p^{II} = \boldsymbol{F}_b^{II} + \nu \Delta \boldsymbol{u}^{II} + \boldsymbol{G}^{II}(\boldsymbol{u}^I), \qquad (1.4a) \\ &\nabla \cdot \boldsymbol{u}^{II} = 0, \qquad (1.4b) \end{aligned}$$

where

$$\boldsymbol{G}^{II}(\boldsymbol{u}^I) \;=\; -((\boldsymbol{u}^I \cdot \nabla)\boldsymbol{u}^I)^{II},$$

for $t \geq t_0$ with

$$\boldsymbol{u}^I(\boldsymbol{x}, t) = \boldsymbol{u}_b^I(\boldsymbol{x}, t), \quad b \in \{A, B, C, D, E\},$$

and with initial data,

$$\boldsymbol{u}^{II}(\boldsymbol{x}, t_0) = 0.$$

We say that the large scale $\boldsymbol{u}_b^I$ reproduces the small scale $\boldsymbol{u}_b^{II}(\boldsymbol{x}, t)$ if

$$\boldsymbol{u}_b^{II}(\boldsymbol{x}, t) - \boldsymbol{u}^{II}(\boldsymbol{x}, t) \to 0. \qquad (1.5)$$

The conclusion is that for all b the large scale $\boldsymbol{u}_b^I$ seem to reproduce the small scale, furthermore the convergence (1.5) appears to be exponential. The rate of convergence depends strongly on the number of modes k_c used in the definition of the large scale. It does however not seem to be so sensitive to the form of the spectrum. An important question is how the number of modes needed to obtain a certain convergence rate depends on the viscosity. We compare two playback calculations, with the same initial data and forcing functions but with different viscosity $\nu = 1/150$ and $\nu = 1/300$. For the small viscosity we obtain a certain convergence rate in L_2 norm sense with $k_c = 13$. We then chose k_c for the large viscosity case so that the convergence rate is similar. The number of modes needed for this case is around $k_c = 8.6$. We furthermore observe that the relative amount of enstrophy contained in the large scale is smaller for the small viscosity case than the large viscosity case for similar convergence rate. The relative amount of kinetic energy contained in the large scale, however is about the same.

To further investigate the possibility to reproduce the small scale from the time-history of the large scale we also perturb the time history. In Section 4 we calculate the solution to (1.4) for $t \geq t_0$ with

$$\boldsymbol{u}^I(\boldsymbol{x}, t) = \boldsymbol{u}_A^I(\boldsymbol{x}, t) + \tilde{\boldsymbol{u}}(\boldsymbol{x}, t), \quad t > t_0$$

with initial data,

$$\boldsymbol{u}^{II}(\boldsymbol{x}, t_0) = 0.$$

Here $|||\tilde{\boldsymbol{u}}||| \approx \epsilon |||\boldsymbol{u}_A^I|||, \quad \epsilon \ll 1$. We make two types of perturbations. The first type has the effect that the magnitude of the Fourier coefficients of $\boldsymbol{u}_A^I(\boldsymbol{x}, t)$ are changed but the phase is not, and the second type has random phase and a spectrum form that is approximately equal to $\epsilon E_{\boldsymbol{u}_b^I}(k)$. The conclusion from the calculations are the same for the two types of perturbations, the small scale is reproduced down to a certain level that can be credited the perturbation, i.e.

$$\lim_t |||\boldsymbol{u}_b^{II}(\boldsymbol{x}, t) - \boldsymbol{u}^{II}(\boldsymbol{x}, t)||| = O(\epsilon).$$

2 Base-runs

In this section five calculations are presented. We solve the equations (1.1) with the same random phase initial data $\boldsymbol{u}_0$ and with four different forcing

functions,

$$\boldsymbol{F} = \boldsymbol{F}_b(\boldsymbol{x}), \quad b \in \{A, B, C\}, \quad \boldsymbol{F} = \boldsymbol{F}_D(\boldsymbol{x}, t),$$

for $\nu = 1/150$ and $N = 128$. The fifth calculation is done with

$$\boldsymbol{F} = \boldsymbol{F}_E(\boldsymbol{x}) = \boldsymbol{F}_A(\boldsymbol{x}),$$

but with $\nu = 1/300$ and $N = 256$. The spectrum of the 0 data is

$$E_{\boldsymbol{u}_0}(k) = C_u k e^{-(k/k_0)^2},$$

where $k_0 = 3.76$ and C_u is chosen such that,

$$\frac{1}{2V}|||\boldsymbol{u}_0|||^2 = \frac{1}{2}.$$

The spectrum of the forcing functions are,

$$E_{\boldsymbol{F}_A}(k) = \tilde{C}_A e^{-(k-3)^2/2}, \ k \geq 1, \tag{2.1}$$

$$E_{\boldsymbol{F}_B}(k) = \tilde{C}_B e^{-(k-5)^2/2}, \ k \geq 1, \tag{2.2}$$

$$E_{\boldsymbol{F}_C}(k) = \tilde{C}_C \frac{k^2}{3^{2+5/3} + k^{2+5/3}} e^{-k^{4/3}/21}, \ k \geq 1, \tag{2.3}$$

$$E_{\boldsymbol{F}_D}(k) = \tilde{C}_D e^{-(k-3)^2/2}, \ k \geq 1, \tag{2.4}$$

and $E_{\boldsymbol{F}_b}(0) = 0$ for $b \in \{A, B, C, D\}$. The constants $\tilde{C}_b$ are chosen such that,

$$\frac{1}{V}|||\boldsymbol{F}_b|||^2 = C_b.$$

The phases of the forcing functions are chosen randomly. For each wave number $\boldsymbol{k} = (k_1, k_2, k_3)^T$ and each forcing function three random uniformly distributed numbers $\Psi_i^b \in [0, 2\pi)$, $i = 1, 2, 3$ are used. For the function $\boldsymbol{F}_D$ above we use,

$$\Psi_1^D(\boldsymbol{k}, t) = \Psi_1^A(\boldsymbol{k}) + \pi sin(3.5\pi^{1/2} f_1 t), \tag{2.5}$$

$$\Psi_2^D(\boldsymbol{k}, t) = \Psi_2^A(\boldsymbol{k}) + \pi sin(4.0\pi^{1/3} f_2 t), \tag{2.6}$$

$$\Psi_3^D(\boldsymbol{k}, t) = \Psi_3^A(\boldsymbol{k}) + \pi sin(3.0\pi^{2/3} f_3 t), \tag{2.7}$$

as the random numbers where Ψ_i^A are the random numbers used for F_A. We chose

$$f_1 = 1.0, \ f_2 = 0.9, \ f_3 = 0.8.$$

These numbers are chosen on the basis that the change in the flow, due to the forcing function, should be comparable to the convergence rate of (1.5). For the calculations the parameters in Table 1 are valid. The kinetic energy and rate of dissipation are estimated in a region where we consider the solution to be pseudo-stationary, this region is here taken as $t \in [10.0, 15.0]$ for $b \in \{A, B, C\}$. For the case D the energy and rate of dissipation varies more due to the time-dependence of the forcing function. For this case we take $t \in [4.0, 9.0]$. For the small viscosity calculation case E we take $t \in [6.0, 8.0]$. The smallest scale is as before estimated based on,

$$\lambda^*_{min} = \sqrt{\frac{\nu}{\overline{|\xi^y_b|_{max}}}}, \quad \overline{|\xi^y_b|_{max}} = \max_t |\xi^y_b|_{max},$$

where ξ^y_b is the y component of the vorticity vector. We argue that the solution is isotropic and therefore that our conclusions based only on ξ^y_b is valid for the whole solution. In Figure 6 - 8 contour plots of ξ^y_b are shown in planes

$$y = y_j = (j-1)(4\pi/3N),$$

at $t = 10.0$ for $b = A, ..., D$. In Figure 1 - 5 the spectrum $E_{\boldsymbol{u}_b}(k)$ and the enstrophy spectrum $k^2 E_{\boldsymbol{u}_b}(k)$ are plotted for the base-runs at $t = t_0$. We argue that the contour plots of ξ^y_b and the plots of the spectrums are representative for the base-runs in the whole time interval of consideration. See also the time study of kinetic energy, rate of dissipation and $|\xi^y_b|_{max}$ in Figure 9 - 13.

3 Playback calculations

In this section we use the large scale of the base-runs from the previous section to make playback calculations, that is experiments with the small scale equations (1.4), according to the introduction. We make playback calculation in the time interval

$$t \in [t_0, t_1],$$

and use different k_c in the definition of the large/small scale, c.f. [1]. The playback-runs are denoted by playback-b, and by

$$\boldsymbol{u}^{II}_{pb,b}(\boldsymbol{x}, t), \quad b \in \{A, B, C, D, E\}.$$

We compare the playback-run to the base-run in $y = y_j$ planes for which $|\xi_b^y|$ attains its maximum. We compute the 2D relative L_2 norm squared

$$\|(\xi_b^y)^{II} - (\xi_{pb,b}^y)^{II}\|^2 / \|\xi_b^y\|^2$$

as well as 2D relative max-norm,

$$|(\xi_b^y)^{II} - (\xi_{pb,b}^y)^{II}|_{max} / |\xi_b^y|_{max}.$$

Table 2, 3 shows these norms for the playback computations. It is clear from Table 2 that the convergence rate is strongly dependent on the number of modes k_c used in the definition of the large scale. A natural question is now how the number of modes needed to obtain a certain convergence rate depends on the viscosity parameter ν ? The playback-E differ to the playback-A essentially in the viscosity. In Figure 14 we have made a least square linear fit to the logarithm of the relative L_2 norms found in the Table 2 and Table 3 for playback-A and $k_c = 8, 9$ and for playback-E and $k_c = 13$. We have not used the data for the playback-E and $t = 7.96$, which we argue is misleading. We believe that this glitch in the otherwise monotone decay is due to the fact that the solution is poorly resolved. By linear interpolation between the slopes of the two playback-A straight lines we find that to obtain the same slope and thereby the same convergence rate (in the L_2 sense) as for playback-E with $k_c = 13$ one would need a $k_c \approx 8.6$.

If we introduce the cumulative kinetic energy and the cumulative enstrophy,

$$\begin{aligned} \mathcal{E}_K &= \sum_{k=0}^{K} E(k), \quad \mathcal{E} = \sum_k E(k), \\ \Omega_K &= \sum_{k=1}^{K} k^2 E(k), \quad \Omega = \sum_k k^2 E(k) \end{aligned}$$

we note from Table 4 that the fraction of kinetic energy in the large scale is about the same for base-run-A, $k_c = 8.6$ and base-run-E, $k_c = 13$. However the fraction of the enstrophy for the small scale is larger for the base-run-E, $k_c = 13$ than for base-run-A and $k_c = 8.6$.

4 Perturbations to a playback calculation

In this section we make perturbations to the large scale time-history $\boldsymbol{u}_A^I$ and ask what happens with the playback procedure. Indeed we can, as will be seen below, still reconstruct the small scales except for a part that can be credited the perturbation.

We solve (1.4) with

$$\boldsymbol{u}^I(\boldsymbol{x},t) = \boldsymbol{u}_A^I(\boldsymbol{x},t) + \tilde{\boldsymbol{u}}(\boldsymbol{x},t), \quad t > t_0, \quad \tilde{\boldsymbol{u}}(\boldsymbol{x},t_0) = 0$$

and

$$\boldsymbol{u}^{II}(\boldsymbol{x},t_0) = 0.$$

Two different perturbations are used here,

1. change of the amplitude of the large scale but not the phase,

$$\hat{\tilde{\boldsymbol{u}}}(\boldsymbol{k},t) = \epsilon \hat{\boldsymbol{u}}_A^I(\boldsymbol{k},t)(cos(2\pi k_1/8) - cos(2\pi k_2/8) + sin(2\pi k_3/8)),$$

2. random phase perturbation,

$$\hat{\tilde{\boldsymbol{u}}}(\boldsymbol{k},t) = \epsilon \hat{\boldsymbol{w}}(\boldsymbol{k}),$$

where $\epsilon \ll 1$. The second perturbation satisfies the incompressibility constraint and for the spectrum it holds that

$$\begin{aligned} E_{\boldsymbol{w}}(k) &\approx E_{\boldsymbol{u}_A^I}(k), \quad k \leq k_c + 1/2, \\ E_{\boldsymbol{w}}(k) &= 0, \quad k > k_c + 1/2. \end{aligned}$$

The spectrum $E_{\boldsymbol{u}_A^I}$ is time-dependent but changes very little during the time interval of the simulation. We denote the solutions to the perturbed playback-runs,

$$\boldsymbol{u}_{pbp,i}^{II}(\boldsymbol{x},t), t \geq t_0,$$

where $i = 1, 2$ is the perturbation type. Perturbed playback-runs are made with

$$t \in [10, 15], \quad t_0 = 10,$$

for $i = 1, \epsilon = 0.005$ and for $i = 2, \epsilon = 0.005, 0.05$. In Table 5 the norms of the difference between the perturbed playback-run and the base-run-A are

shown for the two types of perturbations. For practical reasons the following norms are computed,

$$\frac{||\tilde{\xi^y}||^2 + ||(\xi_A^y)^{II} - (\xi_{pbp,i}^y)^{II}||^2}{||\xi_A^y||^2},$$

and

$$\frac{|(\xi_A^y)^{II} - (\xi_{pbp,i}^y)^{II} - \tilde{\xi^y}|_{max}}{|\xi_A^y|_{max}}.$$

It seems like the small scales are reproduced down to a certain level that depends linearly on the perturbation size parameter ϵ.

Acknowledgment

We would like to thank Dr. Richard Lau at the Office of Naval Research for all the support he has given us over the years. We would like to thank Prof. Arne Johansson for letting us use their computer program and PhD student Krister Alvelius for helping us get started with the code, both at the Department of Mechanics at the Royal Inst. of Technology in Stockholm Sweden. We gladly acknowledge many stimulating discussions with Dr. William Henshaw at Los Alamos National Laboratory and Dr. Gerald Browning at CIRA, Colorado State University and NOAA Forecast System Laboratory. All calculations presented here are done at the DoD High Performance Computing Center, Naval Oceanographic Office(NAVO) MSRC on their Cray C916 PVP system. The post processing is done with ©Matlab v5.1.

References

[1] H-O. Kreiss and J. Yström. A numerical study of the solution to the 3d incompressible navier-stokes equations. Technical Report CAM 98-24, Dep. Mathematics University of California, Los Angeles, 1998.

b	$\boldsymbol{F}$	C_b	ν	N	Δt	$\lambda^*_{min} k^G_{max}$	$\frac{1}{2V}\|\|\|\boldsymbol{u}_b\|\|\|^2$	$\frac{1}{V}\|\|\|\boldsymbol{\xi}_b\|\|\|^2$
A	$\boldsymbol{F}_A$	0.4	1/150	128	0.0018	0.64	0.94-0.99	0.32-0.35
B	$\boldsymbol{F}_B$	0.4	1/150	128	0.0018	0.90	0.41-0.44	0.25-0.27
C	$\boldsymbol{F}_C$	0.4	1/150	128	0.0018	0.90	0.61-0.63	0.21-0.22
D	$\boldsymbol{F}_D$	6.0	1/150	128	0.0018	0.58	0.38-1.00	0.19-0.36
E	$\boldsymbol{F}_A$	0.4	1/300	256	0.0010	0.64	0.92-0.96	0.34-0.36

Table 1: Parameters and data for base-runs.

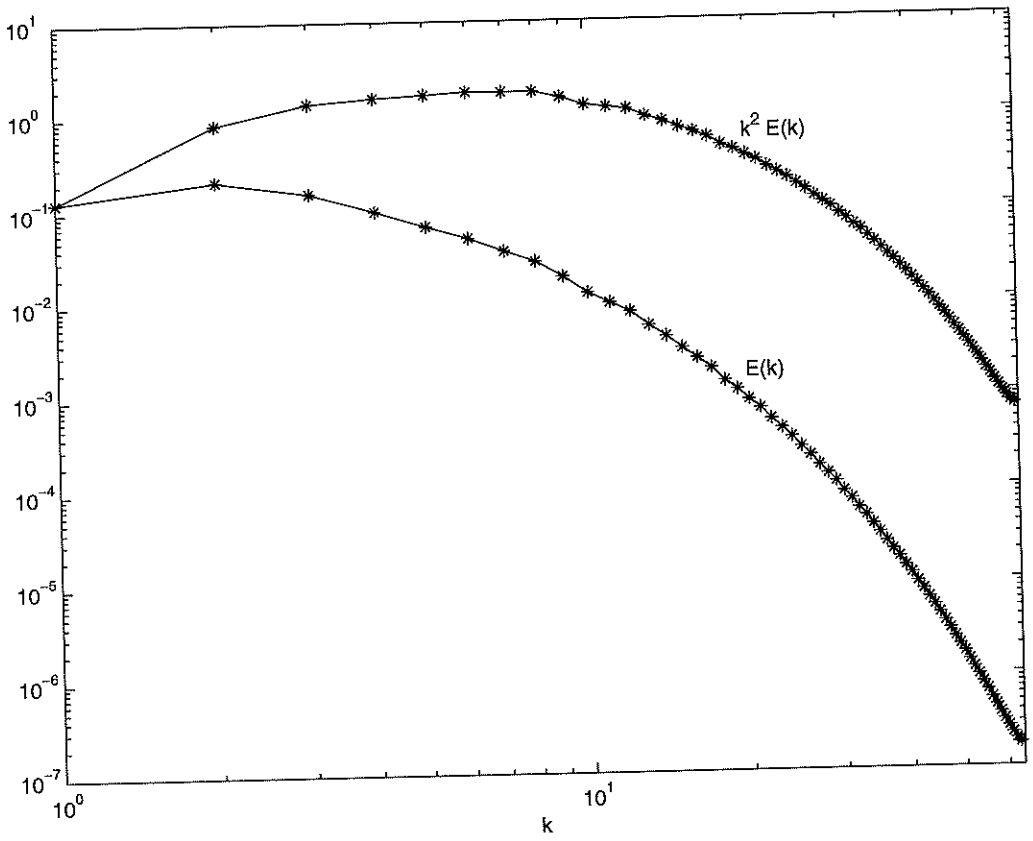

Figure 1: 3D kinetic energy spectrum and enstrophy spectrum for base-run-A at $t = t_0 = 10.0$

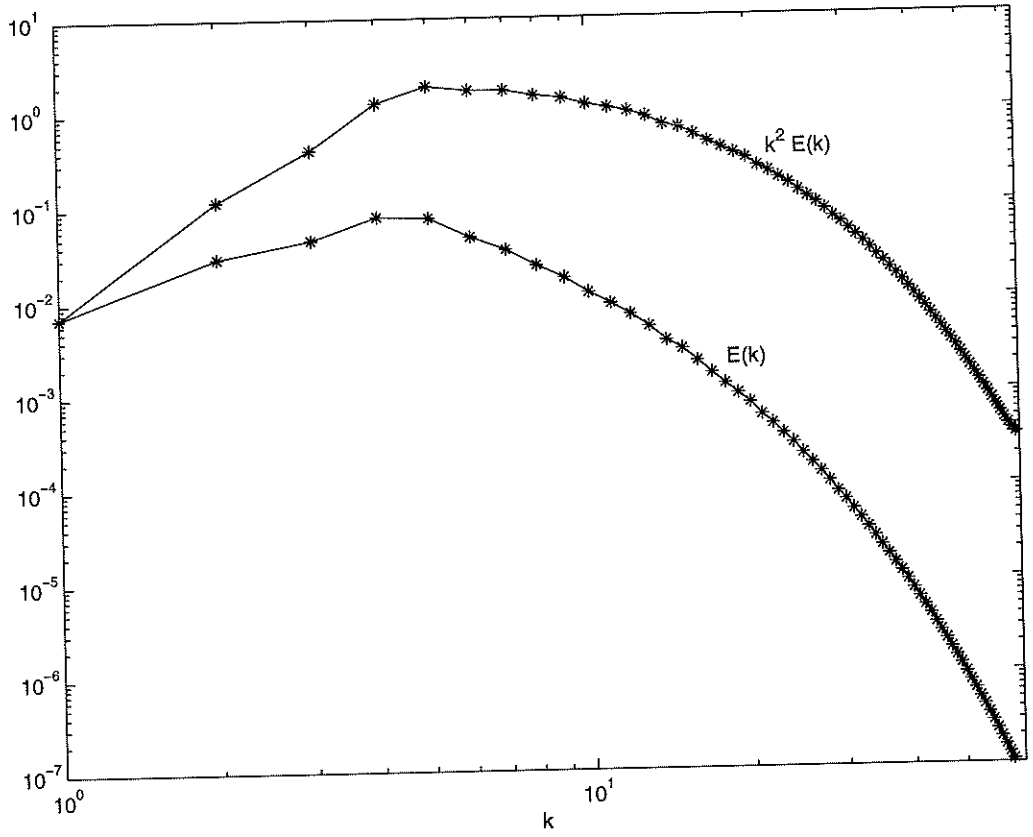

Figure 2: 3D kinetic energy spectrum and enstrophy spectrum for base-run-B at $t = t_0 = 10.0$

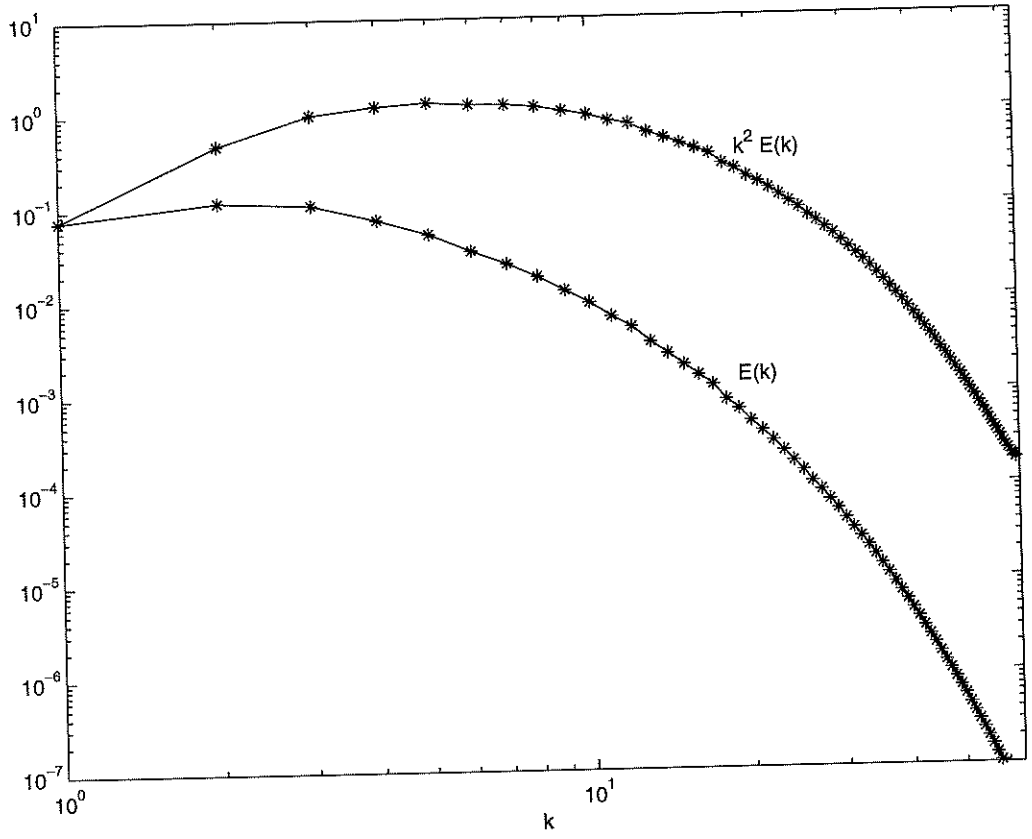

Figure 3: 3D kinetic energy spectrum and enstrophy spectrum for base-run-C at $t = t_0 = 10.0$

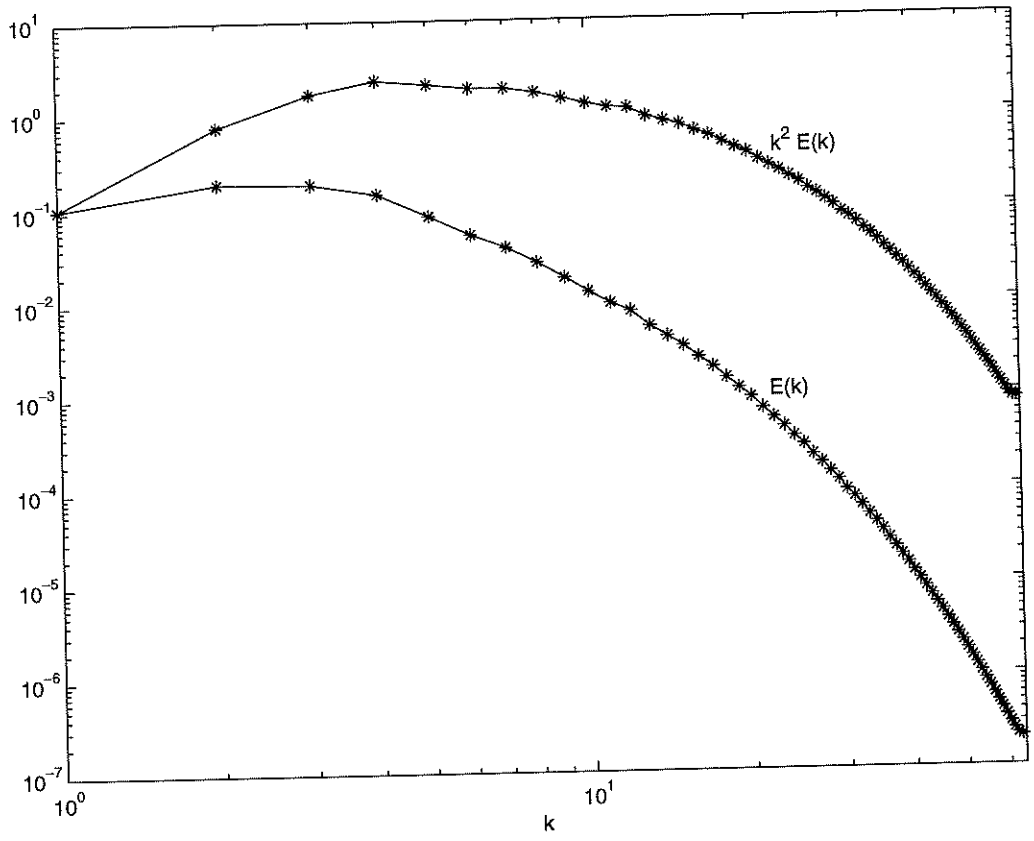

Figure 4: 3D kinetic energy spectrum and enstrophy spectrum for base-run-D at $t = t_0 = 4.0$

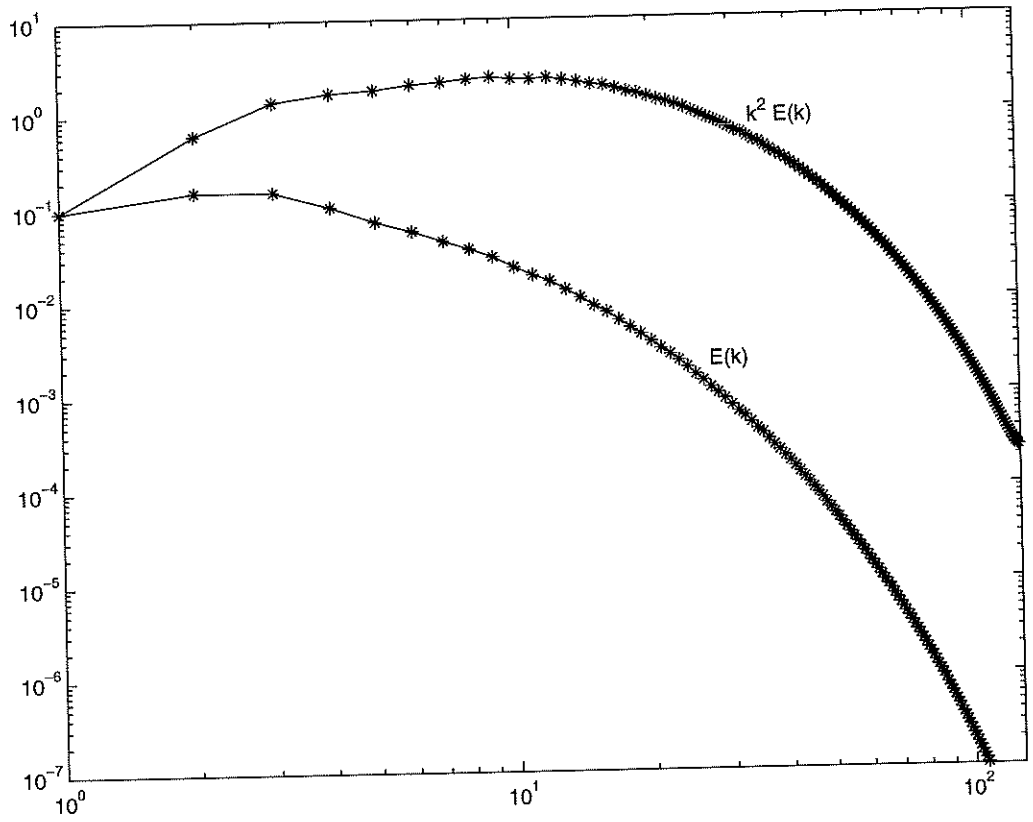

Figure 5: 3D kinetic energy spectrum and enstrophy spectrum for base-run-E at $t = t_0 = 6.0$

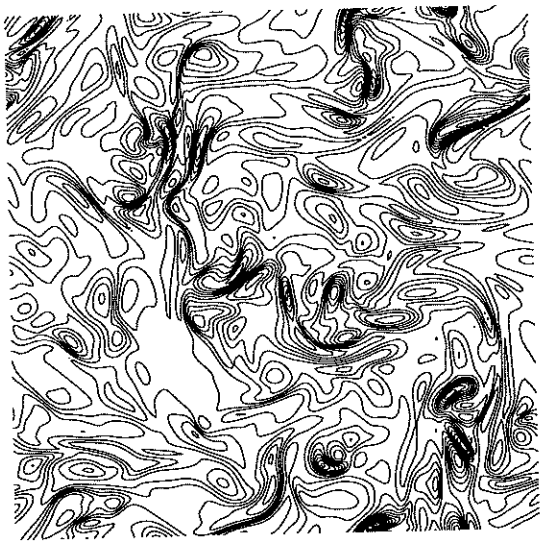

(a) (min,max): $(-30.9, 16.3)$

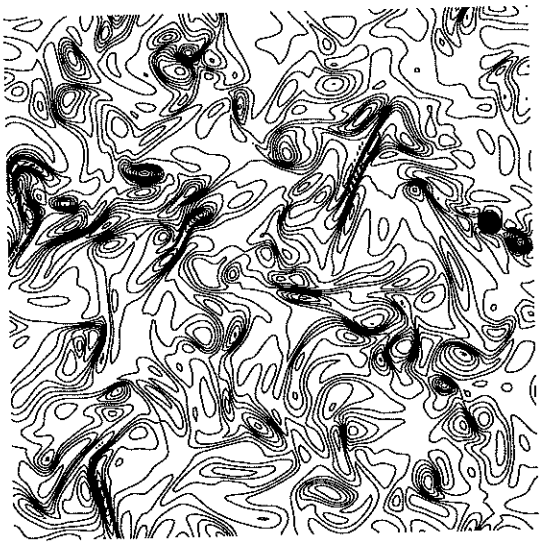

(b) (min,max): $(-30.7, 18.1)$

Figure 6: Contour plots of the y component of the vorticity at $t = t_0 = 10.0$, (a) base-run-A for $y = y_{181}$ and (b) base-run-B for $y = y_{60}$, contour spacing:2

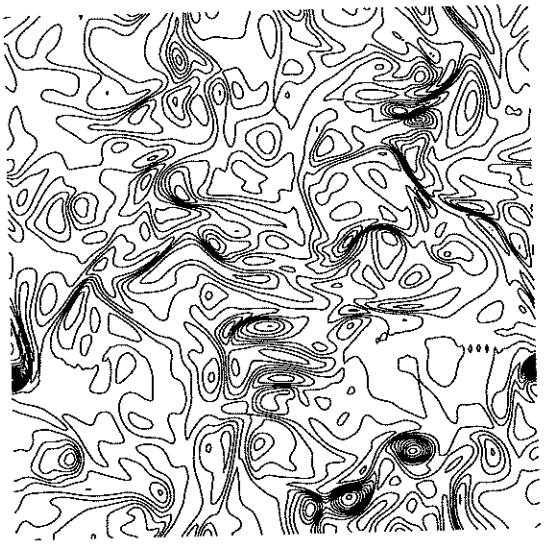

(a) (min,max): $(-32.7, 13.4)$

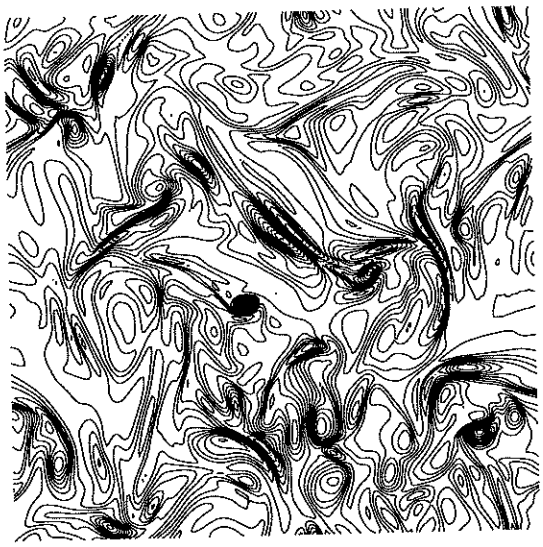

(b) (min,max): $(-21.6, 42.0)$

Figure 7: Contour plots of the y component of the vorticity, (a) base-run-C for $y = y_{110}$ at $t = t_0 = 10.0$, and (b) base-run-D for $y = y_{181}$ at $t = t_0 = 4.0$, contour spacing:2

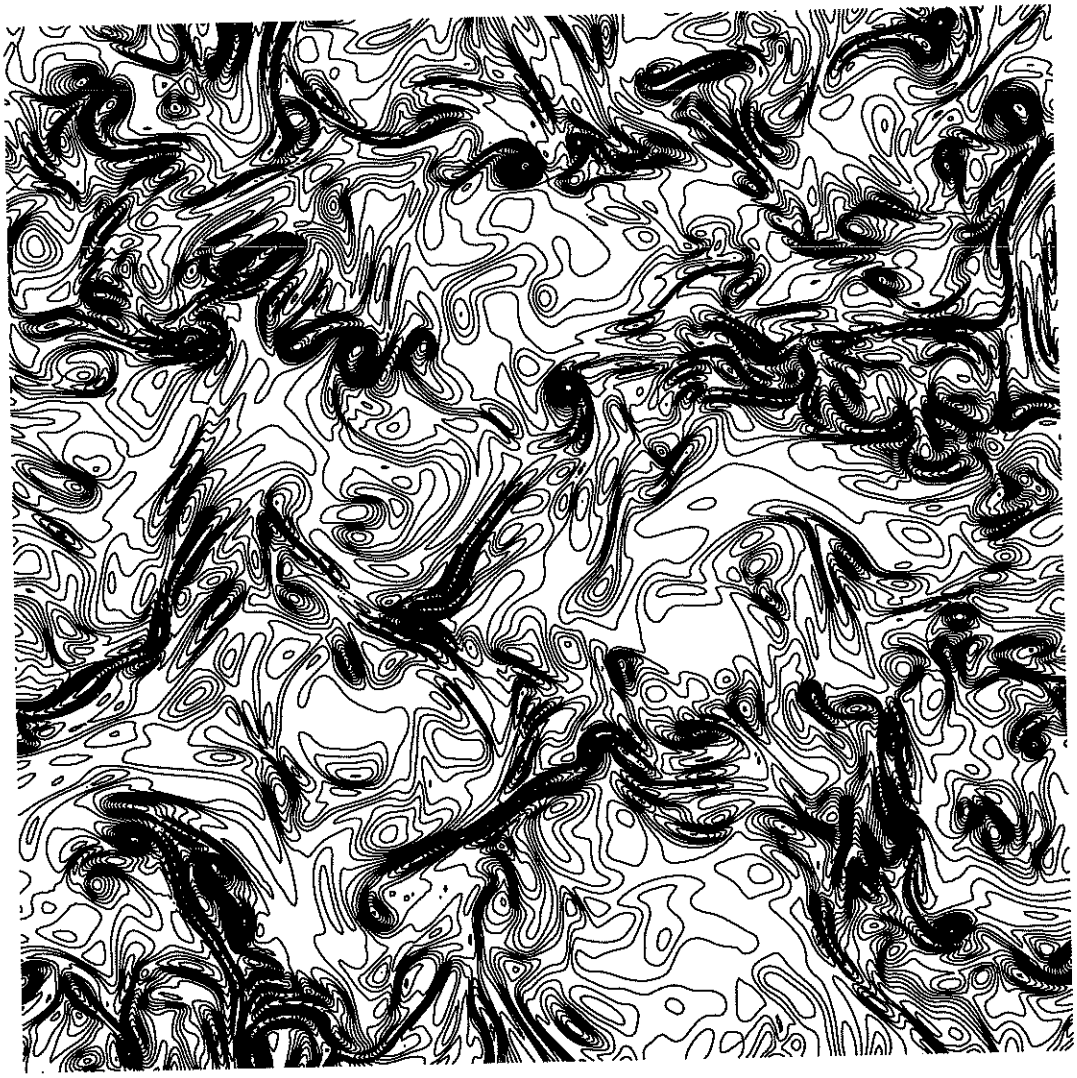

Figure 8: Contour plots of the y component of the vorticity, base-run-E for $y = y_{60}$ at $t = t_0 = 6.0$, (min,max)=(-41.8,79.8), contour spacing:2

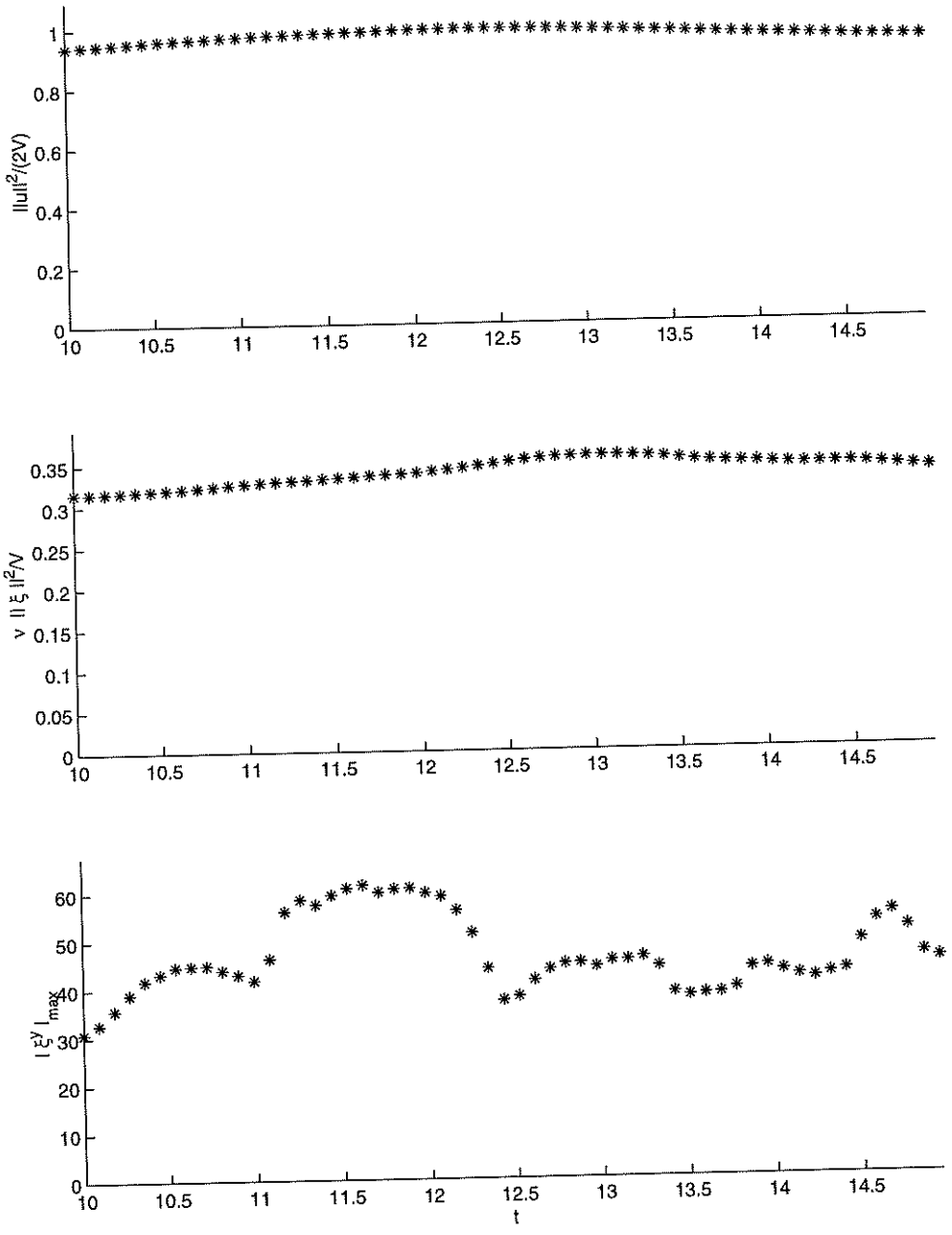

Figure 9: Base-run-A: kinetic energy per unit volume(top), rate of dissipation per unit volume and $|\xi_A^y|_{max}$(bottom)

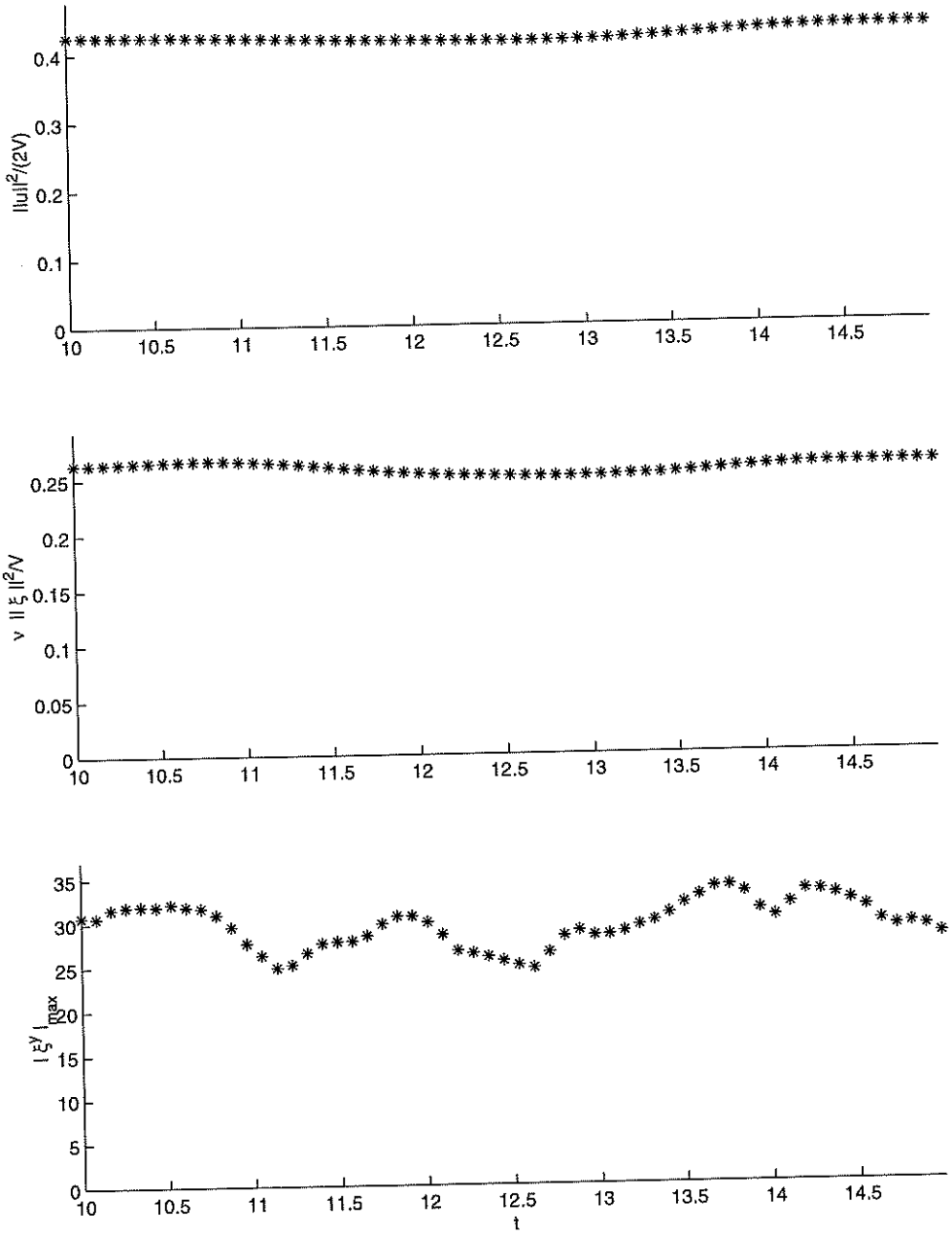

Figure 10: Base-run-B: kinetic energy per unit volume(top), rate of dissipation per unit volume and $|\xi_B^y|_{max}$(bottom)

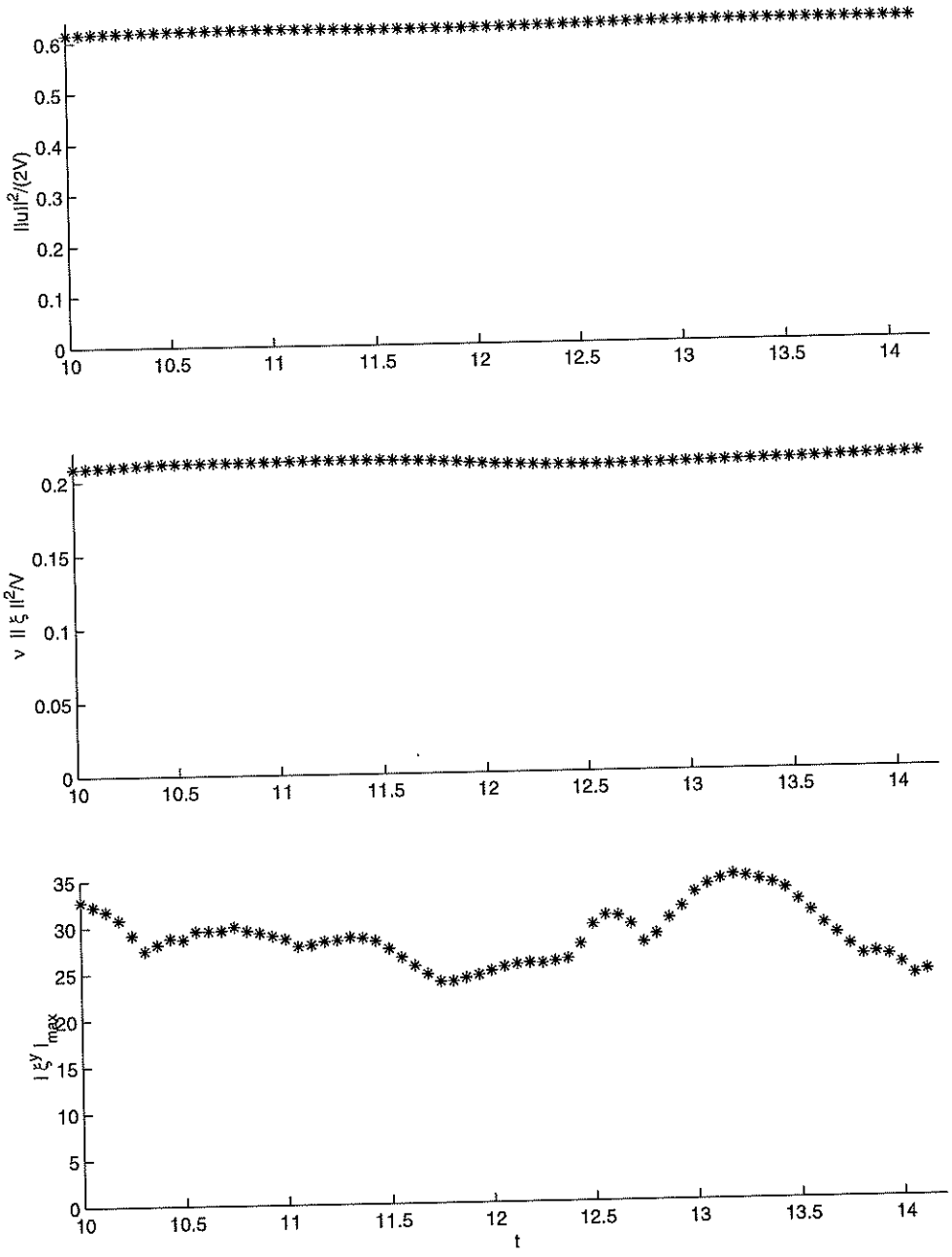

Figure 11: Base-run-C: kinetic energy per unit volume(top), rate of dissipation per unit volume and $|\xi_C^y|_{max}$(bottom)

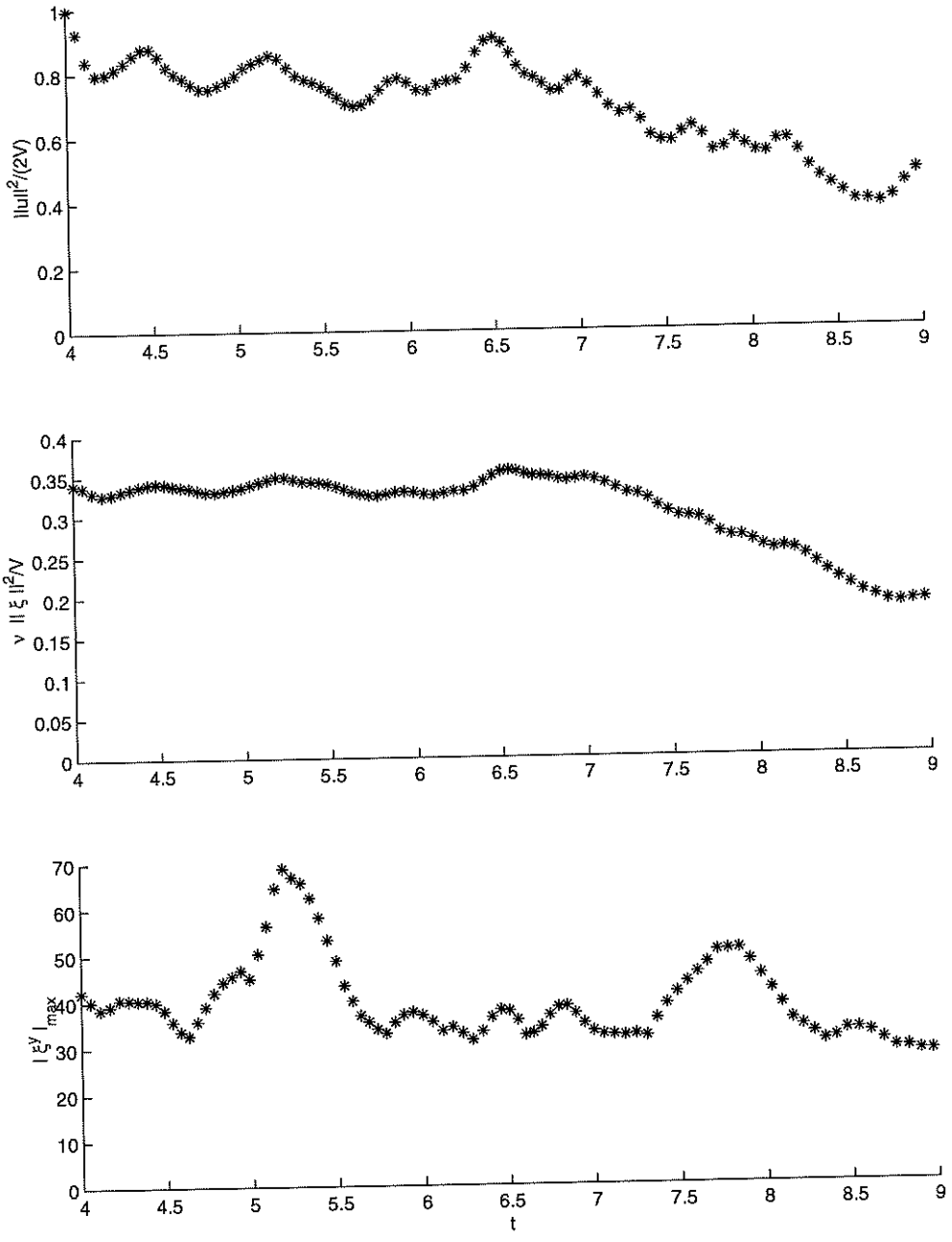

Figure 12: Base-run-D: kinetic energy per unit volume(top), rate of dissipation per unit volume and $|\xi_D^y|_{max}$(bottom)

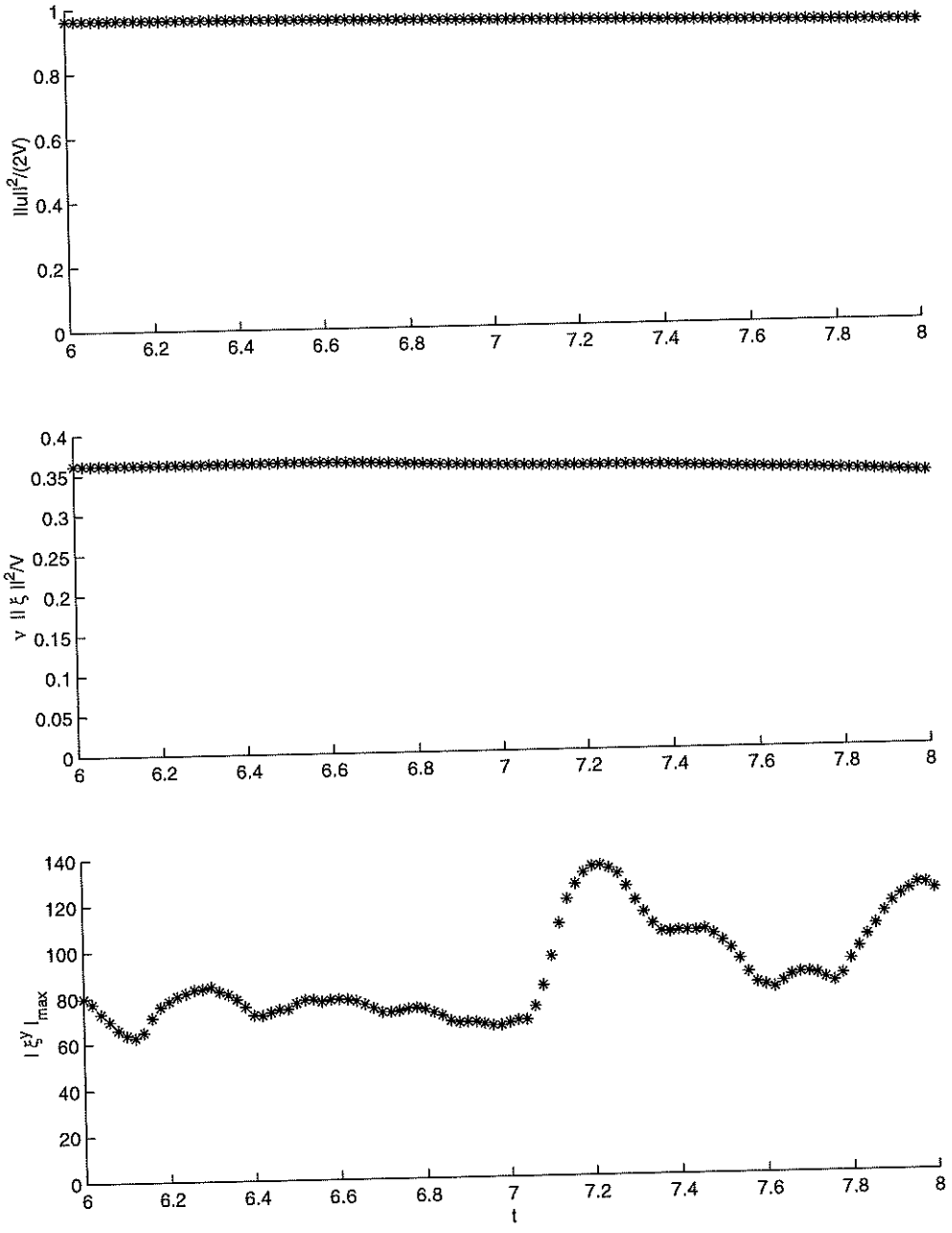

Figure 13: Base-run-E: kinetic energy per unit volume(top), rate of dissipation per unit volume and $|\xi_E^y|_{max}$(bottom)

k_c	y	t	$\frac{\|(\xi_A^y)^{II}-(\xi_{pb,A}^y)^{II}\|^2}{\|\xi_A^y\|^2}$	$\frac{\|(\xi_A^y)^{II}-(\xi_{pb,A}^y)^{II}\|_{max}}{\|\xi_A^y\|_{max}}$
8	y_{181}	10.0	0.4870	0.7563
8	y_{38}	10.45	0.3545	0.5286
8	y_{44}	10.9	0.1785	0.2863
8	y_{158}	11.35	0.1564	0.5912
8	y_{174}	11.8	0.0998	0.6494
8	y_{189}	12.25	0.0499	0.4685
8	y_{68}	12.7	0.0238	0.1904
8	y_{78}	13.15	0.0163	0.2030
8	y_{151}	13.6	0.0087	0.1733
8	y_{91}	14.05	0.0091	0.1563
8	y_{157}	14.5	0.0052	0.2028
9	y_{181}	10.0	0.4066	0.7056
9	y_{38}	10.45	0.2262	0.3821
9	y_{44}	10.9	0.0939	0.2018
9	y_{158}	11.35	0.0755	0.5450
9	y_{174}	11.8	0.0331	0.3008
9	y_{189}	12.25	0.0093	0.0989
12	y_{181}	10.0	0.2749895	0.581207
12	y_{38}	10.45	0.0631647	0.246864
12	y_{44}	10.9	0.0121517	0.075742
12	y_{158}	11.35	0.0033211	0.066540
12	y_{174}	11.8	0.0006282	0.031804
12	y_{189}	12.25	0.0001111	0.013332
12	y_{68}	12.7	0.0000189	0.004972
12	y_{78}	13.15	0.0000034	0.001376
12	y_{151}	13.6	0.0000007	0.000523
12	y_{91}	14.05	0.00000016	0.000540
12	y_{157}	14.5	0.00000003	0.000090

Table 2: Norms for the playback-A calculations

b	k_c	y	t	$\frac{\|\|(\xi_b^y)^{II}-(\xi_{pb,b}^y)^{II}\|\|^2}{\|\|\xi_b^y\|\|^2}$	$\frac{\|(\xi_b^y)^{II}-(\xi_{pb,b}^y)^{II}\|_{max}}{\|\xi_b^y\|_{max}}$
B	12	y_{60}	10.00	0.335	0.80
B	12	y_{71}	10.875	0.0177	0.194
B	12	y_{100}	11.75	0.00084	0.0206
B	12	y_{73}	12.625	0.000043	0.0060
B	12	y_{177}	13.5	0.0000024	0.0032
B	12	y_{47}	14.375	0.000000097	0.00024
C	12	y_{110}	10.00	0.257	0.562
C	12	y_{126}	10.625	0.027	0.231
C	12	y_{182}	11.25	0.0031	0.038
C	12	y_{179}	11.875	0.00031	0.0126
C	12	y_{165}	12.5	0.000030	0.0057
C	12	y_{175}	13.125	0.000003	0.00098
C	12	y_{60}	13.75	0.00000034	0.00083
D	12	y_{181}	4.0	0.270	0.815
D	12	y_{163}	4.59	0.040	0.348
D	12	y_{184}	5.14	0.0048	0.062
D	12	y_{185}	5.68	0.00068	0.032
D	12	y_{175}	6.29	0.000083	0.013
D	12	y_{36}	6.84	0.000011	0.0028
D	12	y_{59}	7.48	0.0000012	0.00063
D	12	y_{44}	8.15	0.00000014	0.00026
D	12	y_{185}	8.90	0.0000000087	0.000063
E	13	y_{60}	6.0	0.5857	0.91386
E	13	y_{330}	6.28	0.3552	0.67299
E	13	y_{66}	6.56	0.2807	0.77616
E	13	y_{140}	6.84	0.1737	0.39942
E	13	y_{218}	7.12	0.1261	0.38750
E	13	y_{210}	7.40	0.0815	0.20182
E	13	y_{248}	7.68	0.0640	0.39019
E	13	y_{185}	7.96	0.1256	0.73595

Table 3: Norms for the playback-B, playback-C, playback-D, and playback-E calculations

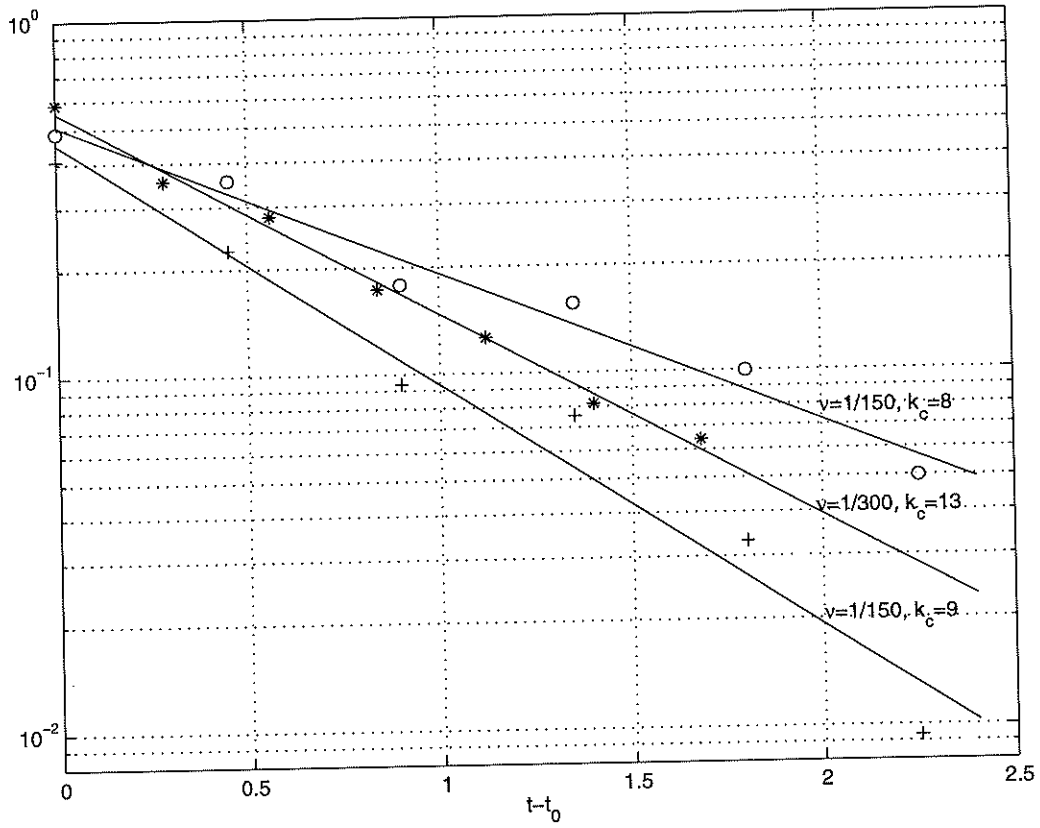

Figure 14: Least-square fit of the logarithm of the L_2 norm decay to a straight line for the playback-A with $k_c = 8, 9$ and the playback-E calculation with $k_c = 13$. The slopes of the straight lines are $-0.97, -1.32, -1.57$.

base-run	k_c	$t - t_0$	$\frac{\mathcal{E}_{k_c}}{\mathcal{E}}$	$\frac{\Omega_{k_c}}{\Omega}$
A	8.6	0.0	0.927	0.514
A	8.6	1.35	0.928	0.510
E	13	0.0	0.924	0.443
E	13	1.4	0.923	0.434

Table 4: Relative energy and enstrophy contents in the large scale for base-run-A, $k_c = 8.6$ and for base-run-E, $k_c = 13$. Here $\mathcal{E}_{8.6} = 0.6\mathcal{E}_9 + 0.4\mathcal{E}_8$ and $\Omega_{8.6} = 0.6\Omega_9 + 0.4\Omega_8$.

i	ϵ	k_c	y	t	$\frac{\|\xi^y\|^2+\|(\xi_A^y)^{II}-(\xi_{pbp,i}^y)^{II}\|^2}{\|\xi_A^y\|^2}$	$\frac{\|(\xi_A^y)^{II}-(\xi_{pbp,i}^y)^{II}-\xi^y\|_{max}}{\|\xi_A^y\|_{max}}$
1.	0.005	12	y_{181}	10.0	0.27499	0.5812
1.	0.005	12	y_{38}	10.45	0.06302	0.2467
1.	0.005	12	y_{44}	10.9	0.01240	0.0758
1.	0.005	12	y_{158}	11.35	0.00355	0.0686
1.	0.005	12	y_{174}	11.8	0.00069	0.0203
1.	0.005	12	y_{189}	12.25	0.00029	0.0193
1.	0.005	12	y_{68}	12.7	0.00024	0.0132
1.	0.005	12	y_{78}	13.15	0.00023	0.0133
1.	0.005	12	y_{151}	13.60	0.00020	0.0154
1.	0.005	12	y_{91}	14.05	0.00025	0.0144
1.	0.005	12	y_{157}	14.5	0.00021	0.0109
1.	0.005	12	y_{87}	14.95	0.00020	0.0171
2.	0.005	12	y_{181}	10.0	0.27499	0.5812
2.	0.005	12	y_{38}	10.45	0.06304	0.2483
2.	0.005	12	y_{44}	10.9	0.01228	0.0767
2.	0.005	12	y_{158}	11.35	0.00360	0.0716
2.	0.005	12	y_{174}	11.8	0.00071	0.0286
2.	0.005	12	y_{189}	12.25	0.00036	0.0312
2.	0.005	12	y_{68}	12.7	0.00020	0.0127
2.	0.005	12	y_{78}	13.15	0.00016	0.0083
2.	0.005	12	y_{151}	13.60	0.00016	0.0213
2.	0.005	12	y_{91}	14.05	0.00018	0.0190
2.	0.005	12	y_{157}	14.5	0.00019	0.0322
2.	0.005	12	y_{87}	14.95	0.00017	0.0189
2.	0.05	12	y_{181}	10.0	0.27499	0.5812
2.	0.05	12	y_{38}	10.45	0.07033	0.2651
2.	0.05	12	y_{44}	10.9	0.02745	0.1859
2.	0.05	12	y_{158}	11.35	0.01922	0.1239
2.	0.05	12	y_{174}	11.8	0.01499	0.1123
2.	0.05	12	y_{189}	12.25	0.02229	0.1953
2.	0.05	12	y_{68}	12.7	0.01756	0.1348
2.	0.05	12	y_{78}	13.15	0.01540	0.0752
2.	0.05	12	y_{151}	13.6	0.01554	0.2436
2.	0.05	12	y_{91}	14.05	0.01781	0.2254
2.	0.05	12	y_{157}	14.5	0.01914	0.3470

Table 5: Norms for perturbed base-run-A